

Elliptic flow of charged hadrons in d+Au collisions at $\sqrt{s_{NN}} = 200$ GeV using a multi-phase transport model

J. Tanwar¹, I. Aggarwal¹, V. Bairathi², L. Kumar¹, and S. Kabana²

¹ Physics Department, Panjab University, Chandigarh, India

² Instituto de Alta Investigación, Universidad de Tarapacá, Casilla 7D Arica 1000000, Chile

Received: date / Revised version: date

Abstract. This study presents a comprehensive analysis of the elliptic flow coefficient, v_2 , for charged hadrons at mid-rapidity in d+Au collisions at $\sqrt{s_{NN}} = 200$ GeV. Utilizing the AMPT model in both default and string melting modes, we examine the dependence of v_2 on transverse momentum, collision centrality, and particle type. Furthermore, we present v_2 scaled by participant eccentricity, which indicates a similar level of collectivity across different centrality intervals in d+Au collisions at $\sqrt{s_{NN}} = 200$ GeV within the AMPT-SM model. Our results indicate that the early-stage partonic phase significantly influences v_2 , as observed by variations in parton scattering cross-section, while the later stage hadronic rescattering shows minimal impact. Comparisons with STAR and PHENIX experimental data show that the AMPT model effectively captures the transverse momentum dependence of v_2 , underlining the importance of parton scattering mechanisms and the need for careful interpretation of experimental results in asymmetric systems.

PACS. 25.75.Ld Collective flow, relativistic collisions

Send offprint requests to: Vipul Bairathi

Correspondence to: vipul.bairathi@gmail.com

1 Introduction

The observation of a hot and dense state of matter, dominated by partonic degrees of freedom, known as Quark-Gluon Plasma (QGP), in high-energy heavy-ion collisions is one of the key discoveries at the Relativistic Heavy Ion Collider (RHIC) and the Large Hadron Collider (LHC) [1, 2, 3, 4]. In non-central heavy-ion collisions, the initial overlap area has an anisotropic energy density profile in the transverse plane that creates pressure gradients, leading to momentum anisotropies of particle distribution relative to the symmetric flow planes, a phenomenon referred to as collective flow [5]. The collective flow can be quantified using flow coefficients derived from the Fourier decomposition of the azimuthal angle distribution of produced particles [6, 7]. Among these, the most commonly studied flow coefficient is the elliptic flow, v_2 .

Several experimental investigations measuring v_2 using various techniques have established the formation of a hydrodynamically expanding QGP medium in heavy-ion collisions [8, 9, 10, 11, 12, 13, 14]. Recent research on heavy-ion collision experiments has gained interest in asymmetric collision systems. At the RHIC, collisions such as p+Au, d+Au, and $^3\text{He}+\text{Au}$ have been performed, while at the LHC, p+Pb collisions have been recorded to further explore and understand the formation of QGP medium in these asymmetric collision systems. Early measurements of v_2 in p+Pb collisions at the LHC [15, 16, 17] and p/d/ $^3\text{He}+\text{Au}$ collisions at RHIC [18, 19, 20, 21, 22] indicate a collective hydrodynamic behavior of the medium produced in these collisions. These findings provide evidence of collectivity in asymmetric collision systems [23]. A recent measurement of v_2 by the STAR collaboration in central p+Au, d+Au, and $^3\text{He}+\text{Au}$ collisions at $\sqrt{s_{\text{NN}}} = 200$ GeV suggest that sub-nucleonic spatial fluctuations, which induce intrinsic deformations in the initial geometry, play a crucial role in the development of the observed azimuthal anisotropies [24].

These studies are effectively described by hydrodynamical models in asymmetric heavy-ion collision systems [22, 25]. Calculations using a multiphase transport (AMPT) model that incorporates both hadronic and partonic scattering can also qualitatively describe the v_2 observed in asymmetric collision systems [26, 27]. In these simulation models, the elliptic anisotropy arises from interactions among medium constituents due to initial collision geometry and fluctuations in sub-nucleonic structure. Alternative explanations for the observed final-state momentum anisotropy, based on initial momentum correlations, have also been proposed [28, 29]. These findings suggest that hydrodynamic-like flow phenomena, typically associated with symmetric nucleus-nucleus collisions, may manifest in asymmetric collision systems under suitable conditions.

In this study, we report the elliptic flow of charged hadrons at mid-rapidity ($|\eta_{\text{cm}}| < 0.9$) in d+Au collisions at $\sqrt{s_{\text{NN}}} = 200$ GeV using the AMPT model. We systematically explore the dependence of $v_2(p_{\text{T}})$ on parton-parton scattering cross-section, hadronic re-scattering time, and different methods of v_2 estimation. Section 2 discusses analysis

methods and briefly describes the AMPT model. Section 3 presents the findings based on these techniques and compares them to available experimental results focusing on asymmetric-system collectivity. Finally, section 4 summarizes and concludes the results.

2 Methodology

This section outlines the model framework and the analysis methods used to calculate the charged hadron elliptic flow in d+Au collisions at $\sqrt{s_{\text{NN}}} = 200$ GeV.

2.1 AMPT model

AMPT is a multi-phase transport model designed to simulate space-time evolution and dynamics of high-energy nuclear collisions [30]. It includes both hadronic and partonic phases, including the hadronization process, which converts partons into hadrons. The AMPT model is mostly used to study collisions involving proton+proton, proton+nucleus, and nucleus+nucleus systems at center-of-mass energies ranging from a few GeV to 200 GeV at RHIC and up to several TeV at the LHC. A good agreement between experimental data and the AMPT model calculations indicates a strong understanding of nucleus-nucleus collisions [21, 31, 32, 33, 34, 35, 36, 37, 38].

The AMPT model consists of four basic components: (1) initial conditions, (2) parton-parton interactions and re-scattering, (3) conversion from partons to hadrons, and (4) interactions among hadrons and hadronic re-scattering. The AMPT model can function in the default mode (AMPT-DEF) and string melting mode (AMPT-SM). The initial conditions of the collisions are generated using the HIJING model through a Monte Carlo Glauber approach. The HIJING model produces minijet partons via hard processes and excited strings through soft processes. The Zhang Parton Cascade (ZPC) model then simulates the partonic interactions and re-scatterings. In the AMPT-DEF mode, partons are recombined with their parent strings following partonic freeze-out and the excited strings are fragmented into hadrons using the Lund string fragmentation model. In AMPT-SM mode, the strings are first melted into partons, and a quark coalescence model is employed to combine all partons into hadrons. Then, the subsequent hadronic interactions and re-scatterings are described using A Relativistic Transport (ART) model. Therefore, the AMPT model provides a convenient way to explore observables in heavy-ion collisions with and without the partonic phase.

In this work, we simulate 100 million minimum bias d+Au collision events at $\sqrt{s_{\text{NN}}} = 200$ GeV using version 2.26t9b of the AMPT model employing both the string melting and default modes. Various input parameters are need to be specified in the model, including parameters a and b in Lund symmetric string fragmentation function,

parton cross-section (σ_{qq}) determined by the QCD coupling constant (α_s) and the parton screening mass (μ), and hadronic rescattering time (t_{had}). The Lund symmetric fragmentation function models hadron production from quark and anti-quark fragmentation, taking into account energy, rapidity, and transverse momentum. A higher value of parameter a results in softer fragmentation with lower mean transverse momentum and higher particle multiplicity. Conversely, a lower value of parameter b indicates higher effective string tension, leading to increased mean transverse momentum for quarks and a higher production of strange quarks relative to non-strange quarks [38]. We used default values of the input parameters, which reasonably described the multiplicity density, particle p_T -spectra, and elliptic flow at $\sqrt{s_{NN}} = 200$ GeV [39, 40]. We also varied these parameters, as listed in Table 1, to systematically study the dependence of v_2 on the parameters σ_{qq} and t_{had} within the AMPT-SM model.

Table 1. Input parameters of the AMPT-SM model.

Parameters	Values	
	Default	Variations
a	0.55	-
b (GeV⁻²)	0.15	-
σ_{qq} (mb)	3.0	1.5, 6.0
t_{had} (fm/c)	30	0.6

The calculation of v_2 in this study is carried out at various centrality intervals. The charged particle multiplicity distribution is used to determine the centrality of an event. This distribution is obtained within a pseudo-rapidity range of $|\eta| < 0.9$ and transverse momentum range of $0.2 < p_T < 3.0$ GeV/ c similar to that in STAR experiment at RHIC [24]. Figure 1 represents the multiplicity distribution for d+Au collisions at $\sqrt{s_{NN}} = 200$ GeV from the AMPT-SM model. The events are categorized into three centrality classes: central (0-10%), mid-central (10-40%), and peripheral (40-80%).

2.2 Flow Analysis Method

The anisotropic flow can be quantified through Fourier decomposition of the azimuthal angle distribution of produced particles with respect to the symmetric collision plane, expressed as follows:

$$\frac{dN}{d\phi} \propto 1 + \sum_n 2v_n \cos[(n(\phi - \psi_n))], \quad (1)$$

where ϕ denotes the azimuthal angle of the produced particles and ψ_n represents the angle of the n^{th} -order symmetric plane of a collision event. The coefficients v_n characterize the strength of anisotropy for each harmonic order n . The

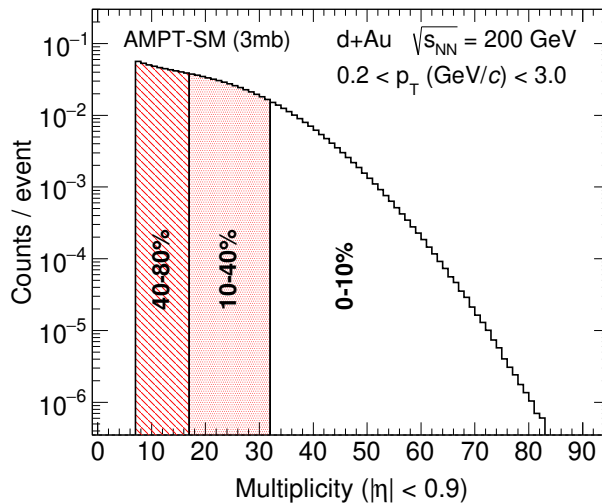


Fig. 1. (Color online) Charged particle multiplicity distribution at mid-rapidity ($|\eta| < 0.9$) in d+Au collisions at $\sqrt{s_{\text{NN}}} = 200$ GeV from the AMPT-SM model. Different bands show selection of 0–10%, 10–40%, and 40–80% collision centrality.

second-order coefficient, v_2 , referred to as elliptic flow, reflects the hydrodynamic response to the initial spatial energy density distribution produced in the early stages of the collision [6, 7].

In this study, we use η -sub event plane method to evaluate v_2 of charged hadrons in d+Au collisions at $\sqrt{s_{\text{NN}}} = 200$ GeV [7]. We begin with the reconstruction of event plane angle, ψ_2 , in two different sub-events comprised of charged hadrons within a negative pseudorapidity range ($-1.8 < \eta < -1.0$) and a positive pseudorapidity range ($1.0 < \eta < 1.8$) and transverse momentum range of $0.2 < p_{\text{T}} < 2.0$ GeV/ c , following the approach outlined in Ref. [24] by the STAR experiment at RHIC. We then obtain v_2 as a function of p_{T} for charged hadrons at mid-rapidity ($|\eta| < 0.9$) with respect to the event plane angle derived from opposite pseudorapidity hemispheres as,

$$v_2^{obs} = \langle \cos[2(\phi - \psi_2)] \rangle, \quad (2)$$

where $\langle \rangle$ denotes average over all particles in all events and ϕ is the azimuthal angle of the particle. An η -gap between calculated v_2 and ψ_2 is applied to reduce non-flow effects due to the short-range correlations. Furthermore, since ψ_2 is reconstructed from a limited number of produced particles, we correct the observed v_2 for the η -sub event plane angle resolution as,

$$v_2 = v_2^{obs} / R_2. \quad (3)$$

Here $R_2 = \sqrt{\langle \cos[2(\psi_2^{\eta^+} - \psi_2^{\eta^-})] \rangle}$, is the η -sub event plane angle resolution. Figure 2 shows second-order η -sub event plane angle resolution as a function centrality in d+Au collisions at $\sqrt{s_{\text{NN}}} = 200$ GeV from the AMPT-SM model. The resolution increases from peripheral to central collisions, as it depends on the particle multiplicity.

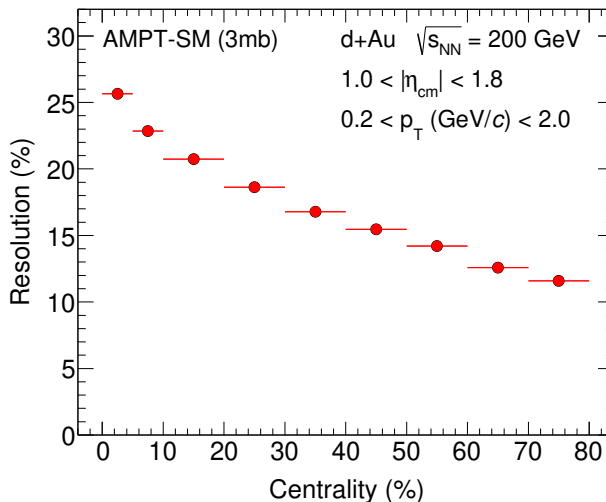


Fig. 2. (Color online) Event plane angle resolution as a function of centrality using the η -sub event plane method in d+Au collisions at $\sqrt{s_{NN}} = 200$ GeV from the AMPT-SM model.

Due to finite number and fluctuations in the positions of nucleons within the colliding nuclei, the initial collision geometry varies event by event. As a result, the participant plane angle may not necessarily align with the true symmetry plane of the collision. These initial geometric fluctuations can lead to the development of elliptic flow. We also calculated v_2 relative to the participant plane angle, denoted as $\psi_2\{\text{pp}\}$. The participant plane angle is obtained event-by-event using transverse positions (r, ϕ) of the participating nucleons in the center of mass frame [41].

3 Results

3.1 Transverse momentum dependence of v_2

We evaluated v_2 as a function of p_T for inclusive charged hadrons (h^\pm) and identified hadrons (π^\pm, K^\pm , and $p(\bar{p})$) at mid-rapidity in 0-80% central d+Au collisions at $\sqrt{s_{NN}} = 200$ GeV. The results are obtained from the AMPT-SM model with a parton-parton cross-section set at 3 mb. Figure 3 shows v_2 calculated with respect to the η -sub event plane and participant plane angles. The $v_2\{\text{ep}\}$ shows a clear monotonic increase with increasing p_T , suggesting a growing contribution of collective motion. In contrast, the $v_2\{\text{pp}\}$ values gradually increase till $p_T \sim 2.0$ GeV and then shows a saturation at higher p_T . The $v_2\{\text{ep}\}$ exhibits a significantly larger magnitude across all identified particles and inclusive charged hadrons than the $v_2\{\text{pp}\}$ values. The $v_2\{\text{pp}\}$ is determined using the event plane angle calculated from the participating nucleons in the initial state. Therefore, $v_2\{\text{pp}\}$ reflects initial anisotropy in particle production arising from the initial geometric configuration of the collision, providing insight into the anisotropy driven by the

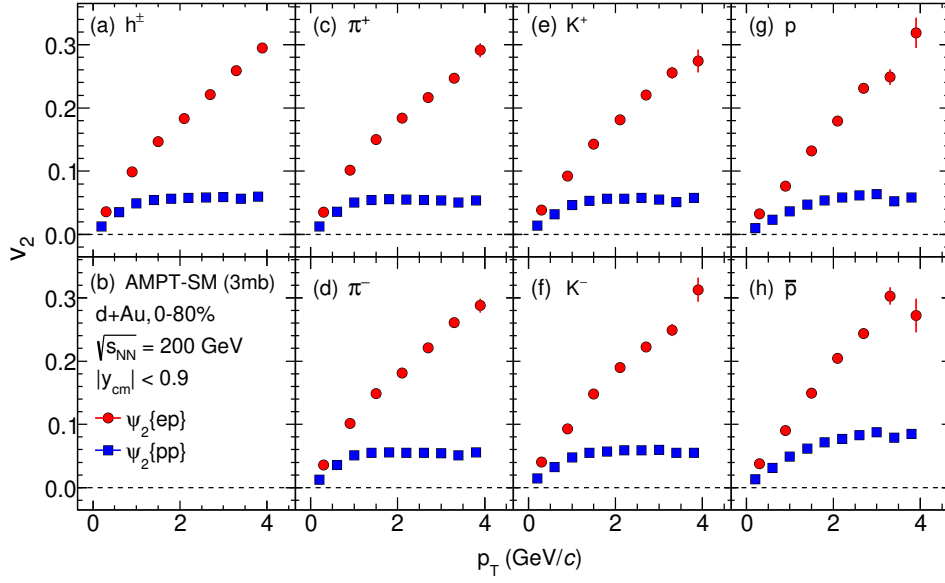


Fig. 3. (Color online) v_2 as a function of p_T for inclusive charged hadrons and identified hadrons at mid-rapidity in 0–80% central d+Au collisions at $\sqrt{s_{NN}} = 200$ GeV from the AMPT-SM model. The statistical uncertainties are indicated by the error bars.

initial spatial eccentricity of the system. Moreover, the difference between $v_2\{ep\}$ and $v_2\{pp\}$ indicates the contribution of momentum anisotropy developed during the final stages of the system’s evolution.

3.2 Centrality dependence of v_2

The shape of colliding nuclei and initial collision geometry in heavy-ion collisions influence the expansion and dynamics of the produced medium. The centrality of a collision depends on the initial collision geometry and the shape of colliding nuclei. Studying the centrality dependence of v_2 is important, as it can provide insights into the properties of the produced medium, thermalization processes, and hydrodynamic behavior [9]. Therefore, we studied the centrality dependence of elliptic flow by computing charged and identified hadron $v_2(p_T)$ in three centrality classes (0-10%, 10-40%, and 40-80%) for d+Au collisions at $\sqrt{s_{NN}} = 200$ GeV using the AMPT-SM model. In Fig. 4, we present v_2 as a function of p_T with respect to η -sub event plane and participant plane angle. We observed a weak centrality dependence of $v_2\{ep\}$ in d+Au collisions at $\sqrt{s_{NN}} = 200$ GeV, in contrast to heavy-ion collisions, where a clear centrality dependence has been reported [9, 42, 43, 46].

We further investigate the influence of initial collision geometry on elliptic flow in d+Au collisions at $\sqrt{s_{NN}} = 200$ GeV by calculating participant eccentricity (ε_{2p}) scaled v_2 . The eccentricity is obtained as described in Ref. [41]. This scaling removes the effects of initial collision geometry on the elliptic flow and thus provides insight into the degree

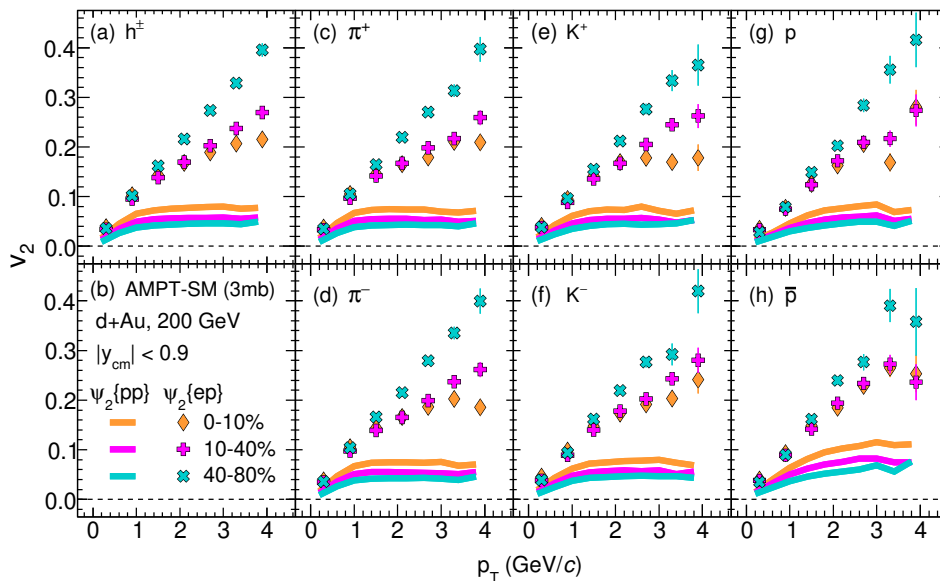


Fig. 4. (Color online) v_2 as function of p_T for inclusive charged and identified hadrons at mid-rapidity d+Au collisions at $\sqrt{s_{NN}} = 200$ GeV from the AMPT-SM model. The statistical uncertainties are indicated by the error bars.

of collectivity of the produced thermalized medium. In Fig. 5, we present v_2/ε_{2p} as a function of p_T for inclusive charged and identified hadrons in d+Au collisions at $\sqrt{s_{NN}} = 200$ GeV for centrality 0-10%, 10-40%, and 40-80%. The results from the AMPT-SM model indicate that the order of collectivity observed across different centrality ranges is similar in d+Au collisions at $\sqrt{s_{NN}} = 200$ GeV as opposed to heavy-ion collisions, where higher collectivity is associated with central collisions compared to the peripheral collisions [9, 42, 43, 46].

3.3 Particle type dependence of v_2

The elliptic flow of identified hadrons in Au+Au collisions at $\sqrt{s_{NN}} = 200$ GeV has been extensively studied at RHIC [3, 4]. Large values and centrality dependence of v_2 , consistent with hydrodynamic model calculations, have been reported [47, 48, 49]. The study of particle type dependence of v_2 provides valuable insight into the mechanism of particle production in high-energy nuclear collisions. Particle mass ordering of the v_2 at low p_T (< 2.0 GeV/ c) and baryon-meson separation at intermediate p_T (2-5 GeV/ c) suggests a collective expansion of the medium and hadronization through quark coalescence, respectively [43].

We present $v_2(p_T)$ of π^+ , K^+ , and p at mid-rapidity in d+Au collisions at $\sqrt{s_{NN}} = 200$ GeV for various centrality classes: 0-80%, 0-10%, 10-40%, and 40-80% using the AMPT-SM model. The results are shown in Fig. 6 (left) for v_2 calculated with respect to the η -sub event plane and participant plane angle. There is no significant particle mass

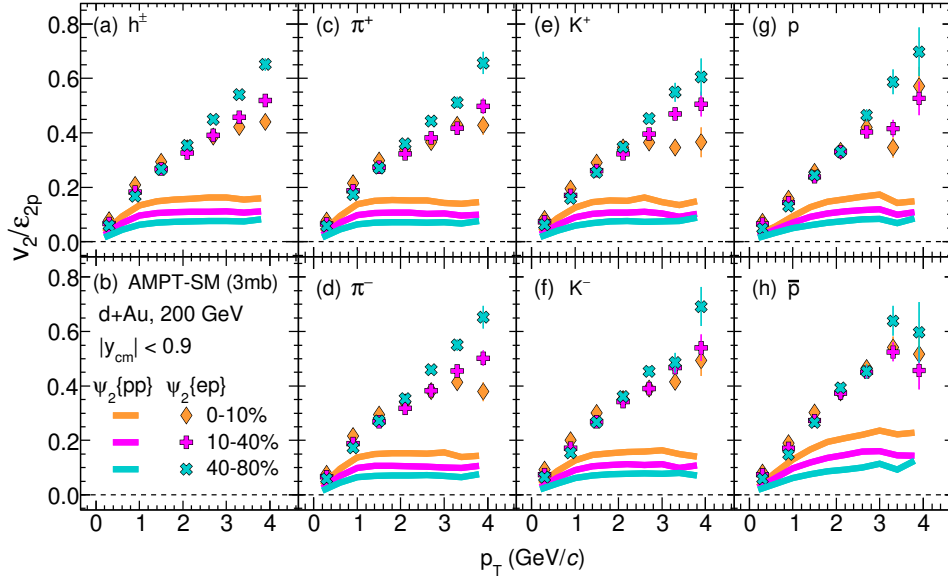


Fig. 5. (Color online) v_2/ε_{2p} as function of p_T for inclusive charged and identified hadrons at mid-rapidity d+Au collisions at $\sqrt{s_{NN}} = 200$ GeV from the AMPT-SM model. The statistical uncertainties are indicated by the error bars.

ordering at low p_T , nor any evident baryon-meson separation at intermediate p_T observed, for all centrality classes in d+Au collisions at $\sqrt{s_{NN}} = 200$ GeV.

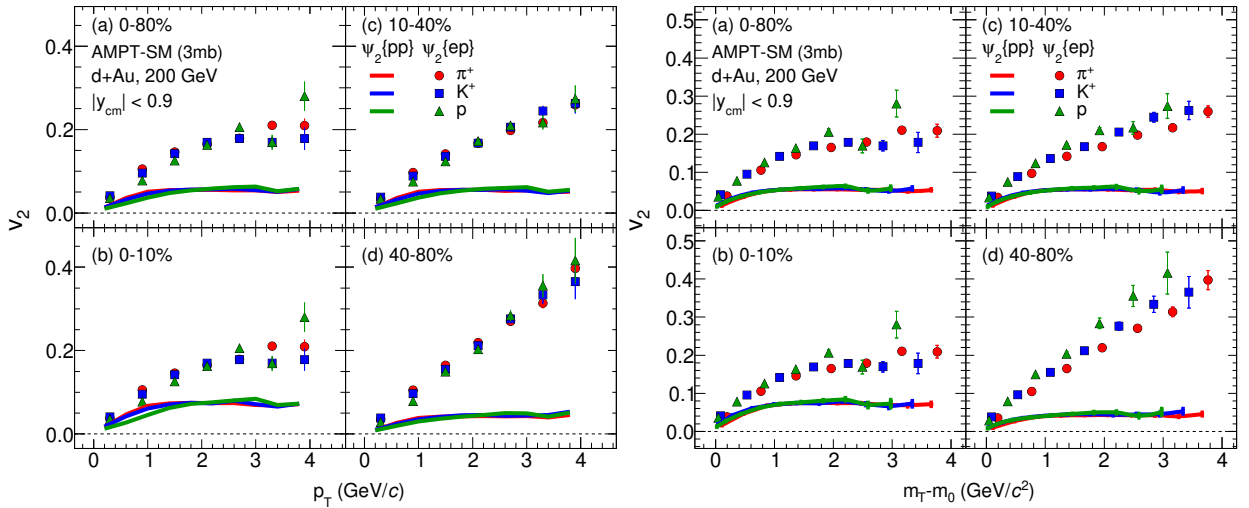


Fig. 6. (Color online) v_2 of π^+ , K^+ , and p as a function of p_T (left) and $m_T - m_0$ (right) for centrality (a) 0-80%, (b) 0-10%, (c) 10-40%, and (d) 40-80% in d+Au collisions at $\sqrt{s_{NN}} = 200$ GeV from the AMPT-SM model. The error bars represent statistical uncertainties.

We further investigated the identified hadron v_2 as a function of transverse kinetic energy ($KE_T = m_T - m_0$) in Fig. 6 (right) to examine the baryon-meson separation in d+Au collisions at $\sqrt{s_{NN}} = 200$ GeV. Here, m_T and m_0 represent the transverse mass and rest mass of the particles, respectively. This representation is particularly useful for removing the dependence of particle mass on flow measurements. We observed that v_2 plotted against KE_T does not show a clear separation between baryon-meson v_2 , in contrast to the symmetric heavy-ion collisions [9]. The absence of particle species-dependent behavior suggests that the medium created in small collision systems, such as d+Au, may not be dominated by the partonic contribution. These findings imply that the mechanisms driving anisotropic flow in small asymmetric systems could be qualitatively different from those observed in symmetric heavy-ion collisions.

The number of constituent quark (NCQ) scaling of elliptic flow reflects the collective behavior of de-confined partons in the early stages of heavy-ion collisions, and it is typically interpreted within the framework of parton recombination or coalescence models [50, 51, 52]. In previous studies at RHIC, the scaling of v_2 with the number of constituent quarks has been observed in symmetric heavy-ion collisions at beam energies ranging from $\sqrt{s_{NN}} = 7.7$ to 62.4 GeV [32, 42]. However, at top RHIC energy ($\sqrt{s_{NN}} = 200$ GeV), there are indications of deviations from the NCQ scaling behavior [43, 44]. Similar deviations have also been observed at the LHC in larger systems like Pb+Pb collisions at $\sqrt{s_{NN}} = 2.76$ TeV, where the high parton density can disrupt conditions necessary for the coalescence mechanism [45]. This suggests that NCQ scaling is not a strict requirement for coalescence at high quark densities. Nonetheless, it remains feasible to examine NCQ in smaller asymmetric systems.

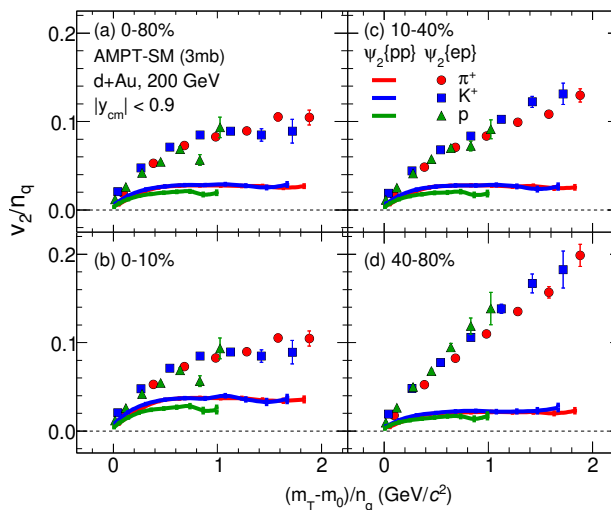


Fig. 7. (Color online) The NCQ scaled v_2 as a function of scaled transverse kinetic energy ($m_T - m_0/n_q$) for π^+ , K^+ , and p in (a) 0-80%, (b) 0-10%, (c) 10-40%, and (d) 40-80% in d+Au collisions at $\sqrt{s_{NN}} = 200$ GeV from the AMPT-SM model. The error bars represent statistical uncertainties.

In Fig. 7, we present v_2 of π^+ , K^+ , and p scaled by the number of constituent quarks (n_q) as a function of KE_T/n_q for various centrality classes in d+Au collisions at $\sqrt{s_{NN}} = 200$ GeV from the AMPT-SM model. Our analysis shows that while we observe NCQ scaling, the results do not adequately explain the associated baryon-meson splitting of v_2 in d+Au collisions at this energy.

3.4 Partonic and hadronic scattering dependence of v_2

The AMPT model, which incorporates both initial state partonic scatterings and final state hadronic cascading, has been shown to describe collective flow coefficients measured in heavy-ion collisions at RHIC and the LHC. Therefore, the input parameters for parton-parton scattering cross-section and hadronic cascading time in the AMPT model are crucial to understand how hadronization through string fragmentation and quark coalescence mechanism and the subsequent hadronic cascade impact the v_2 in asymmetric systems.

In this study, we report charged hadron v_2 in d+Au collisions at $\sqrt{s_{NN}} = 200$ GeV using the AMPT-SM model with varying parton-parton cross sections (1.5 mb, 3.0 mb, and 6.0 mb), along with the AMPT-DEF model. Figure 8 shows charged hadron v_2 calculated with respect to the η -sub event plane and participant plane angles with different values of parton scattering cross-sections. We observed that the magnitude of v_2 increases with increasing parton scattering cross-section, reflecting stronger partonic collectivity. A larger parton scattering cross-section results in a stronger collective flow signal. This trend is consistent with previous studies in symmetric systems, such as Au+Au and Pb+Pb collisions.

The results from the AMPT model are compared to experimental measurements at mid-rapidity for 0-10% central d+Au collisions at $\sqrt{s_{NN}} = 200$ GeV from the STAR experiment at RHIC [24]. We observe that the v_2 calculated with respect to the η -sub event plane angle ($\psi_2\{\text{ep}\}$), for all parton scattering cross-section values, overestimates the STAR experimental data. However, v_2 calculated with respect to the $\psi_2\{\text{pp}\}$ from the AMPT-DEF model and parton scattering cross-sections of 6 mb from the AMPT-SM model are consistent with the experimental measurements within the uncertainties. Note that the charged hadron v_2 from the STAR experiment is measured with the two particle azimuthal angle correlation method, while we use event plane method in the AMPT model.

In Fig. 8, we also compared our results from the AMPT model with experimental measurements at mid-rapidity for 0-5% central d+Au collisions at $\sqrt{s_{NN}} = 200$ GeV from the PHENIX experiment at RHIC [23]. The PHENIX results are obtained using the η -sub event plane method which provide a critical benchmark for testing flow sensitivity to initial geometry and non-flow suppression techniques. The v_2 calculated with respect to the η -sub event plane from

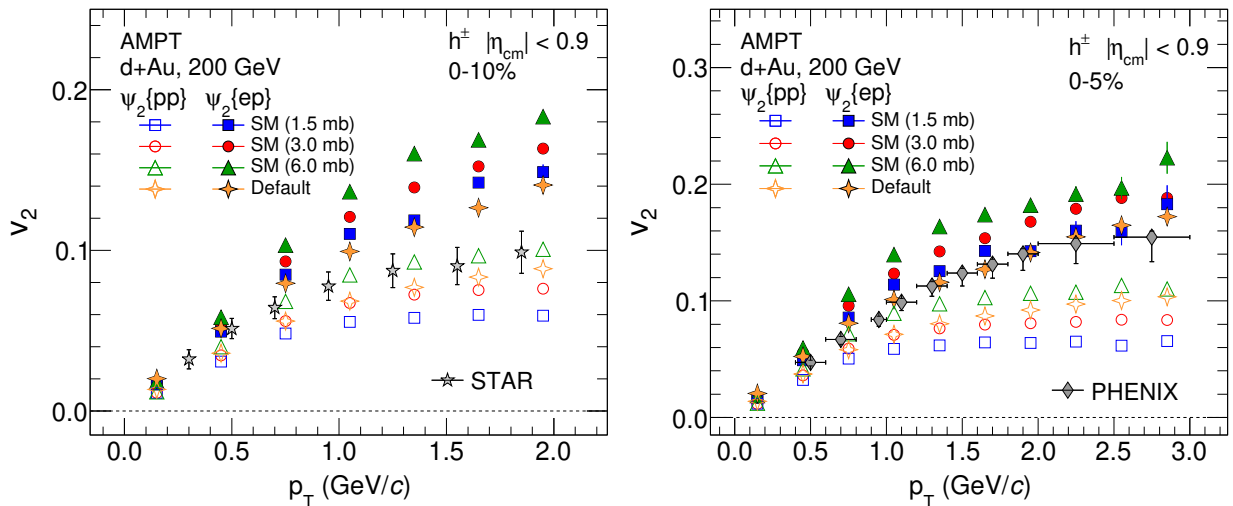


Fig. 8. (Color online) $v_2(p_T)$ of charged hadrons at mid-rapidity in 0–10% (left) and 0–5% (right) central d+Au collisions at $\sqrt{s_{NN}} = 200$ GeV from the AMPT model. The results of charged hadrons v_2 from the STAR and PHENIX experiment at RHIC in same collision system and energy are also shown. Statistical uncertainties are indicated by the error bars.

the AMPT-DEF model and parton scattering cross-sections of 1.5 mb from the AMPT-SM model are well describe the experimental measurements within the uncertainties.

In Fig. 9, we show a comparison of charged hadron $v_2(p_T)$ at mid-rapidity in 0–10% central d+Au collisions at $\sqrt{s_{NN}} = 200$ GeV with varying hadron cascading times (0.6 and 30 fm/c) and fixed parton scattering cross-section (3 mb) using the AMPT model. This allows us to examine the effect of final-state hadronic interactions and re-scatterings on the calculated v_2 . The charged hadron v_2 shows a weak dependence and changes slightly with increasing hadron cascading time, indicating that the final-state hadronic interactions have a negligible impact on the development of azimuthal anisotropy in asymmetric systems.

The AMPT model predictions are also compared with experimental results from the STAR Collaboration [24]. The experimental results lie close to v_2 calculated with respect to the participant plane angle for a hadron cascading time of 30 fm/c using the AMPT model in d+Au collisions at $\sqrt{s_{NN}} = 200$ GeV.

4 Summary and Conclusions

In this study, we present a comprehensive analysis of the elliptic flow coefficient, v_2 , for charged hadrons at mid-rapidity in d+Au collisions at $\sqrt{s_{NN}} = 200$ GeV. We utilize the AMPT model, both in its default and string melting mode. We discuss the dependence of charged hadrons v_2 on particle type, collision centrality, and transverse momentum. To explore the influence of initial conditions, we obtained v_2 with respect to $\psi_2\{pp\}$ and compared it to the results with

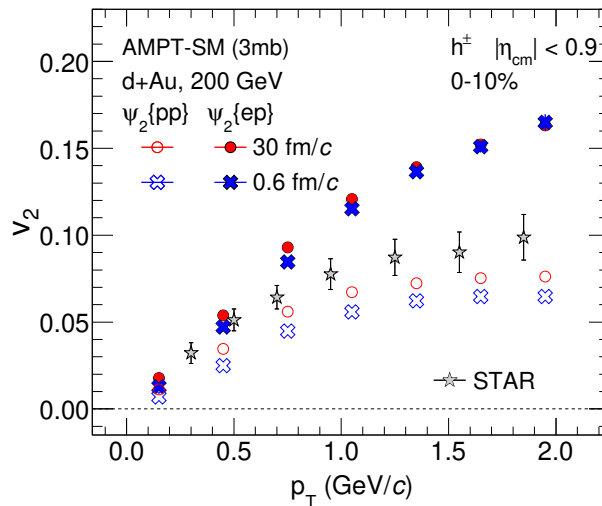


Fig. 9. (Color online) Charged hadron $v_2(p_T)$ at mid-rapidity in 0–10% central d+Au collisions at $\sqrt{s_{NN}} = 200$ GeV from the AMPT model with different hadronic cascading time. The results from the STAR experiment at RHIC in d+Au collisions are also shown using gray star markers. Statistical uncertainties are indicated by the error bars.

respect to $\psi_2\{ep\}$. Additionally, we present v_2 scaled by participant eccentricity, which suggests a similar order of collectivity across different centrality intervals in d+Au collisions at $\sqrt{s_{NN}} = 200$ GeV within the AMPT-SM model.

We systematically examined the effects of early-stage partonic phase and final-state hadron dynamics on the development of azimuthal anisotropy in asymmetric collision systems by varying the parton scattering cross-section and hadronic rescattering time. The results indicate that increasing parton-parton cross-section in the AMPT-SM model enhances the magnitude of v_2 . In contrast, the hadronic rescattering time has a minimal effect on the calculated v_2 for inclusive charged hadrons. This suggests that v_2 predominantly arises from the early-stage partonic phase rather than the later-stage hadronic processes. Our findings highlight the importance of parton scattering mechanisms in shaping the azimuthal anisotropy observed in asymmetric collision systems.

A comparison of charged hadron v_2 in 0-10% central d+Au collisions with experimental data from the STAR collaboration indicates that the AMPT-SM model, with a partonic cross-section of approximately 6.0 mb, shows better overall agreement in reproducing the transverse momentum dependence of v_2 with respect to the participant plane angle. Additionally, a comparison of charged hadron v_2 measured with respect to the event plane angle in 0-5% central d+Au collisions with PHENIX experimental data reveals that the results from both the AMPT-DEF and AMPT-SM models with a small partonic cross-section of 1.5 mb, describe the experimental findings. This discrepancy in v_2 results derived from two different estimation methods highlights the significance of simulations in interpreting experimental results, especially in asymmetric systems where non-flow effects must be carefully considered.

Acknowledgments

LK acknowledges the support of the Research Grant No. SR/MF/PS-02/2021-PU (E-37120) from the Department of Science and Technology, Government of India.

References

1. I. Arsene *et al.* (BRAHMS Collaboration), *Nucl. Phys. A* **757**, 1 (2005).
2. B. B. Back *et al.* (PHOBOS Collaboration), *Nucl. Phys. A* **757**, 28 (2005).
3. J. Adams *et al.* (STAR Collaboration), *Nucl. Phys. A* **757**, 102 (2005).
4. K. Adcox *et al.* (PHENIX Collaboration), *Nucl. Phys. A* **757**, 184 (2005).
5. U. Heinz and R. Snellings, *Ann. Rev. Nucl. Part. Sci.* **63**, 123 (2013).
6. S. A. Voloshin and Y. Zhang *Z. Phys. C* **70**, 665 (1996).
7. A. M. Poskanzer and S. A. Voloshin *Phys. Rev. C* **58**, 1671 (1998).
8. B. Alver *et al.* (PHOBOS Collaboration), *Phys. Rev. Lett.* **98**, 242302 (2007).
9. B. I. Abelev *et al.* (STAR Collaboration), *Phys. Rev. C* **77**, 054901 (2008).
10. B. I. Abelev *et al.* (STAR Collaboration), *Phys. Rev. C* **81**, 044902 (2010).
11. A. Adare *et al.* (PHENIX Collaboration), *Phys. Rev. C* **92**, 034913 (2015).
12. S. Acharya *et al.* (ALICE Collaboration), *J. High Energ. Phys.* **2018**, 103 (2018).
13. S. Acharya *et al.* (ALICE Collaboration), *J. High Energ. Phys.* **2023**, 243 (2023).
14. S. Acharya *et al.* (ALICE Collaboration), *Phys. Lett. B* **846**, 137453 (2023).
15. S. Chatrchyan *et al.* (CMS Collaboration), *Phys. Lett. B* **718**, 795 (2013).
16. B. Abelev *et al.* (ALICE Collaboration), *Phys. Lett. B* **719**, 29 (2013).
17. G. Aad *et al.* (ATLAS Collaboration), *Phys. Rev. Lett.* **110**, 182302 (2013).
18. A. Adare *et al.* (PHENIX Collaboration), *Phys. Rev. Lett.* **111**, 212301 (2013).
19. A. Adare *et al.* (PHENIX Collaboration), *Phys. Rev. Lett.* **114**, 192301 (2015).
20. A. Adare *et al.* (PHENIX Collaboration), *Phys. Rev. Lett.* **115**, 142301 (2015).
21. C. Aidala *et al.* (PHENIX Collaboration), *Phys. Rev. C* **96**, 064905 (2017).
22. C. Aidala *et al.* (PHENIX Collaboration), *Phys. Rev. Lett.* **120**, 062302 (2018).
23. C. Aidala *et al.* (PHENIX Collaboration), *Nat. Phys.* **15**, 214-220 (2019).
24. M. I. Abdulhamid *et al.* (STAR Collaboration), *Phys. Rev. Lett* **130**, 242301 (2023).

25. R. D. Weller and P. Romatschke, *Phys. Lett. B* **774**, 351-356 (2017).
26. P. Bozek, A. Bzdak, and G.-L. Ma, *Phys. Lett. B* **748**, 301-305 (2015).
27. J. D. Orjuela Koop et al., *Phys. Rev. C* **92**, 054903 (2015).
28. K. Dusling and R. Venugopalan, *Phys. Rev. Lett.* **108**, 262001 (2012).
29. A. O. Velasquez et al., *Phys. Rev. Lett.* **111**, 042001 (2013).
30. Z.-W. Lin et al., *Phys. Rev. C* **72**, 064901 (2005).
31. L. Adamczyk et al. (STAR Collaboration), *Phys. Rev. C* **86**, 054908 (2012).
32. L. Adamczyk et al. (STAR Collaboration), *Phys. Rev. C* **88**, 014902 (2013).
33. L. Adamczyk et al. (STAR Collaboration), *Phys. Rev. C* **88**, 014904 (2013).
34. A. Adare et al. (PHENIX Collaboration), *Phys. Rev. C* **94**, 054910 (2016).
35. Y. He and Z.-W. Lin, *Phys. Rev. C* **96**, 014910 (2017).
36. S. Acharya et al. (ALICE Collaboration), *J. High Energ. Phys.* **2018**, 6 (2018).
37. Y. He and Z.-W. Lin, *Eur. J. Phys. A* **56**, 123 (2020).
38. Z.-W. Lin and L. Zheng, *Nucl. Sci. Tech.* **32**, 113 (2021).
39. Z.-W. Lin, *Phys. Rev. C* **90**, 014904 (2014).
40. A. Nandi, L. Kumar, and N. Sharma, *Phys. Rev. C* **102**, 024902 (2020).
41. B. Alver and G. Roland, *Phys. Rev. C* **81**, 054905 (2010) [Erratum *Phys. Rev. C* **82**, 039903].
42. L. Adamczyk et al. (STAR Collaboration), *Phys. Rev. C* **93**, 014907 (2016).
43. M. S. Abdallah et al. (STAR Collaboration), *Phys. Rev. C* **103**, 064907 (2021).
44. A. Adare et al. (PHENIX Collaboration), *Phys. Rev. C* **85**, 064910 (2012).
45. B. B. Abelev et al. (ALICE Collaboration), *J. High Energ. Phys.* **2015**, 6, 190 (2015).
46. T. Bhat et al., *Phys. Lett. B* **859**, 139103 (2024).
47. C. Nonaka, R. J. Fries and S. A. Bass, *Phys. Lett. B* **583**, 73 (2004).
48. T. Hirano and Y. Nara, *Phys. Rev. C* **69**, 034908 (2004).
49. B. Schenke, S. Jeon, and C. Gale, *Phys. Rev. Lett.* **106**, 042301 (2011).
50. D. Molnár and S. A. Voloshin, *Phys. Rev. Lett.* **91**, 092301 (2003).
51. R. J. Fries et al., *Phys. Rev. C* **68**, 044902 (2003).
52. L. Zheng et al., *Eur. Phys. J. A* **53**, 124 (2017).